ATLAS Paper

ATLAS-CONF-2016-XX

Searches for resonant and non-resonant Higgs boson pair-production in the $b\bar{b}\tau^+\tau^-$ decay channel with 36.1 fb^{-1} pp collision data at $\sqrt{s}$ = 13 TeV with the ATLAS detector

The ATLAS Collaboration

20th December 2017

A search for resonant and non-resonant Higgs boson pair-production decaying to a $b\bar{b}\tau^+\tau^-$ final state is presented. The search uses 36.1 fb^{-1} of pp-collision data with $\sqrt{s}$ = 13 TeV recorded by the ATLAS experiment at the LHC in 2015 and 2016. The semi-leptonic and fully hadronic di-tau final states are considered. No deviation from the Standard Model prediction of XXX pb at $\sqrt{s}$ = 13 TeV is observed. The cross-section times branching ratio for non-resonant Higgs pair-production is constrained to be less than XX times the Standard Model prediction. The results are also interpreted in terms of constraints on a Randall-Sundrum Kaluza-Klein graviton model, and a 2HDM model in an extended Higgs sector. Upper limits are placed on the resonant di-Higgs production cross-section times branching ratio for $b\bar{b}\tau^+\tau^-$ final states.

The discovery of a new particle at the Large Hadron Collider (LHC) in 2012 by the ATLAS and CMS collaborations [1, 2] has provided important insight into the mechanism of electroweak symmetry breaking. Electroweak symmetry breaking can be further probed by measurement of the Higgs trilinear self-coupling (λ_{hhh}) through di-Higgs production (h→hh), which provides a direct test of the Standard Model (SM) prediction of the shape of the Higgs potential. In the SM Higgs bosons can be pair-produced both via top loops or the Higgs boson self-interaction. In several extensions of the SM this cross-section can be enhanced. Non-resonant Higgs boson pair-production can be significantly enhanced by modifications to the top Yukawa coupling or the Higgs self-coupling λ_{hhh}, or by introducing new couplings. Other theories predict heavy resonances that could decay to a pair of $m_{\mathrm{h}} = 125$ GeV Higgs bosons, such as a heavy spin-0 scalar, H, in two Higgs doublet models (2HDM) [3] and spin-2 Kaluza Klein (KK) excitations of the graviton G^*_{KK}, in the bulk Randall-Sundrum (RS) model [4, 5].

This letter describes searches for resonant and non-resonant di-Higgs production decaying to a final state with two b-jets and two τ leptons using 36.1 fb^{-1} of data recorded by the ATLAS detector [6] in 2015 and 2016. Both the $\tau_\ell\tau_{\mathrm{had}}$ and $\tau_{\mathrm{had}}\tau_{\mathrm{had}}$ channels are considered, where the subscripts (ℓ=electron or muon, had=hadrons) indicate the decay of the τ leptons. The $b\bar{b}\tau^+\tau^-$ final state[1] has the third largest measurable branching fraction (7.4% [**LHCHIGGXSWG**]) of all di-Higgs decay channels, and provides a relatively clean signature compared to channels with larger branching fractions ($bbbb$ and $bbWW$) due to a more distinct separation from multi-jet and $t\bar{t}$ backgrounds.

A previous search for di-Higgs production in the $bb\tau\tau$ channel was performed by the ATLAS experiment using data collected by the LHC in 2012 with a centre-of-mass energy $\sqrt{s} = 8$ TeV. The analysis used the $\tau_\ell\tau_{\mathrm{had}}$ decay mode to set limits on the production cross-section for resonances with masses in the range 260 GeV $< m_{\mathrm{X}} <$ 1 TeV and to set an upper limit on the SM cross-section for non-resonant di-Higgs production of 1.6 pb (160 times the SM prediction) [7]. The ATLAS combination of this result with the $bbbb$ [8], $bb\gamma\gamma$ [9], and $WW\gamma\gamma$ [7] channels yielded an upper limit on the cross-section for non-resonant di-Higgs production of 0.67 pb (70 times the SM prediction). Searches for resonant and non-resonant Higgs boson pair-production in the $bb\tau\tau$ channel were performed by the CMS experiment using 35.9 fb^{-1} data with $\sqrt{s}$=13 TeV [10] and non-resonant di-Higgs production is excluded for cross-sections greater than 28 times the SM prediction.

Simulated samples of resonant di-Higgs production in Two-Higgs-Doublet Models (2HDM) [3] and the bulk Randall-Sundrum (RS) model in extra dimensions [4, 5] were produced for 14 different mass points between 260 and 1000 GeV. In both cases, the heavy resonance decays into two SM-like Higgs bosons with $m_h = 125$ GeV. The 2HDM model is a gluon-initiated state implemented in MadGraph5 at leading-order (LO) [11] and interfaced to the Pythia 8.186 [12] parton shower model. The A14 tune [13] is used together with the NNPDF2.3LO parton distribution function (PDF) set [14]. The width of the heavy scalar, H, is fixed to 4 MeV. Signal G^*_{KK} events are produced with different values of the coupling constant $c = k/\bar{M}_{\mathrm{Pl}}$ (0.5, 1.0, 2.0). The parameter k corresponds to the curvature of the warped extra dimension and the effective four-dimensional Planck scale $\bar{M}_{\mathrm{Pl}} = 2.4 \times 10^{18}$ GeV. Both the cross-section and natural width depend on c.

Non-resonant di-Higgs samples, assuming a Higgs boson mass of 125.09 GeV and SM production diagrams, are simulated using an effective field theory (EFT) model that includes finite top mass correction through form factors. The model is implemented in MG5_aMC@NLO v2.2.2 [15] at next-to-leading-order (NLO) and interfaced to the Herwig ++ parton shower and hadronisation model [16] and uses the

[1] Throughout this letter the inclusion of charge-conjugate decay modes is implied.

UEEE5 tune and CTEQ6L1 PDF set. The samples are reweighted in order to account for the effects of taking into account the full top-quark mass dependence [17, 18].

For the generation of background $t\bar{t}$ and single top-quarks in the Wt and s-channel the Powheg-Box v2 [19] generator with the CT10 PDF sets in the matrix element calculations is used. Electroweak t-channel single top-quark events are generated using the Powheg-Box v1 generator. This generator uses the 4-flavour scheme for the NLO matrix elements calculations together with the fixed four-flavour PDF set CT10f4. For all top processes, top-quark spin correlations are preserved; for t-channel production, top quarks are decayed using MadSpin [20]. The parton shower, fragmentation, and the underlying event are simulated using Pythia 6.428 [21] with the CTEQ6L1 PDF sets and the corresponding Perugia 2012 tune (P2012) [22]. The top-quark mass is set to 172.5 GeV. The EvtGen v1.2.0 program [23] is used to model the properties of the bottom and charm hadron decays. The $t\bar{t}$ production cross-section is calculated at NNLO+NNLL [24]. For single top processes, the generator NLO cross-sections are used.

Background events containing W or Z bosons with associated jets are simulated using the Sherpa 2.2.1 [25] generator. Matrix elements are calculated for up to 2 partons at NLO and 4 partons at LO using the Comix [26] and OpenLoops [27] matrix element generators and merged with the Sherpa parton shower [28] using the ME+PS@NLO prescription [29]. The CT10NLO PDF set is used in conjunction with dedicated parton shower tuning developed by the Sherpa authors. All W/Z+jets events are normalised to the predicted cross-sections using NNLO calculations.

Background diboson (ZZ, WW, WZ) processes with one of the bosons decaying hadronically and the other leptonically are simulated using the Sherpa 2.1.1 generator [25]. They are calculated for up to one (ZZ) or zero (WW, WZ) additional partons at NLO and up to three additional partons at LO. The CT10 PDF set is used in conjunction with dedicated parton shower tuning developed by the Sherpa authors. The generator NLO cross-sections are used.

Standard Model Higgs production in association with a Z boson, subsequently decaying to a $bb\tau\tau$ final state is an irreducible background to this analysis. The $qqZh(Z \to \tau\tau, h \to bb)$ and $qqZh(Z \to bb, h \to \tau\tau)$ processes are generated with Pythia 8.186 [21], using the A14 tune and NNPDF23LO PDF set. The gluon-fusion initiated $Zh(Z \to \tau\tau, h \to bb)$ process is generated with Powheg-Box v2 [19] using the CT10 PDF sets. The parton shower, fragmentation, and the underlying event are simulated using Pythia 8.186 [21]. The AZNLO [30] tune is used, with PDF set CTEQ6L1, for the modelling of non-perturbative effects. The cross-section of the $qqZh(Z \to bb, h \to \tau\tau)$ process is scaled up by 6% in order to account for its gluon-fusion initiated counterpart, due to difficulties in modelling the gluon-fusion component. For all ZH processes, the EvtGen v1.2.0 program [23] is used to model properties of the bottom and charm hadron decays. Other SM Higgs boson processes were negligible.

All samples are passed through the full GEANT4 [31, 32] simulation of the ATLAS detector and are reconstructed with the same software as used for data.

Events compatible with containing a $\tau\tau bb + E_{\mathrm{T}}^{\mathrm{miss}}$ final state are selected (where $\tau\tau$ includes both the $\tau_\ell\tau_{\mathrm{had}}\tau_{\mathrm{had}}$ and τ_{had} final states).

To select the $\tau_\ell\tau_{\mathrm{had}}$ final state events a logical OR of single lepton and lepton + τ_{had} triggers is used. Electrons are required to pass a minimum p_{T} requirement between 18 and 27 GeV. They must also pass requirements on the shape of the cluster of energy deposits in the calorimeter, as well as on track-to-cluster matching and the quality of the track [33]. Electron candidates are identified using a likelihood technique in combination with additional track hit requirements, providing an electron efficiency of 95%. Muons are required to be within $|\eta| < 2.5$ and to have a minimum p_{T} between 15 and 27 GeV. Muon tracks

are reconstructed independently in the inner detector (ID) and the muon spectrometer (MS). Tracks are required to have a minimum number of hits in each system, and must be compatible in terms of geometrical and momentum matching. Information from both the ID and MS systems is used in a combined fit to refine the measurement of the momentum of each muon [34]. Isolation requirements in the tracking detectors and calorimeters reject non-prompt muons with typically 99% efficiency independent of p_{T}.

Jets, formed by an anti-k_t algorithm with radius parameter $R = 0.4$ and clusters of calorimeter cells using a local hadronic calibration as inputs, are used as seeds for the visible hadronic τ decay ($\tau_{\text{had-vis}}$) reconstruction algorithm [35] [36] [37] if they satisfy $p_T > 10\,\text{GeV}$ and $|\eta| < 2.5$, excluding the barrel-endcap transition region of the calorimeter ($1.37 < |\eta| < 1.52$). A multi-variate Boosted Decision Tree (BDT) discriminant, using variables based on information about the tracks and energy deposits in the calorimeter around the $\tau_{\text{had-vis}}$ candidate as inputs, provides discrimination between hadronically decaying taus and other jets. An additional multivariate likelihood is used to distinguish between 1-track hadronically decaying taus and electrons.

To select the $\tau_{\text{had}}\tau_{\text{had}}$ final state a logical OR of single (lead $\tau p_{\mathrm{T}} > 80$-160 GeV) and di-tau (leading (sub-leading) *tau* $p_{\mathrm{T}} > 35$ (25) GeV) triggers is used. The di-tau trigger additionally requires a jet with $p_{\mathrm{T}} > 25\,\text{GeV}$ at Level 1 for data collected during 2016. Selected $\tau_{\text{had-vis}}$ candidates are required to be of at least 'medium' quality, have one or three tracks, unit charge, to be within $|\eta| < 2.3$, and to have a minimum p_{T} between 40 and 180 GeV, depending on the trigger that is being used. τ_{had} candidates with less than 'medium' quality but fulfilling all other requirements are considered in background studies as fake-τ_{had}. The second hadronically decaying $\tau_{\text{had}}$is required to be within $|\eta| < 2.3$ and to have a minimum p_{T} of 20 or 30 GeV.

The missing transverse momentum ($E_{\mathrm{T}}^{\text{miss}}$) is defined as the opposite of the vector sum of the transverse energy of all objects in an event, computed using fully calibrated and reconstructed physics objects. Fake-τ's used for background estimates are treated as tau-like objects in the $E_{\mathrm{T}}^{\text{miss}}$ computation.

In all cases, events with additional electrons, muons or taus are rejected. The visible τ decay products are required to be of opposite-sign charge and have an invariant di-τ mass using the Mass Calculator [38]), $m_{\tau\tau}^{\text{MMC}}$, of $> 60\,\text{GeV}$.

Jets originating from b-quarks are identified using the MV2 multivariate discriminant [39, 40] trained against a background sample containing 10% charm-initiated jets. A working point that corresponds to an average tagging efficiency of 70% for b-jets in $t\bar{t}$ events is used, that provides a rejection factor of around 140 (5) against light (charm) jets.

Events are split into categories according to the multiplicity of b-tagged jets. Only events with exactly two b-tagged jets are considered for the signal region. Events with zero and one b-tagged jets are used as control and validation regions for background estimation. In the one b-tag region the b-tagged jet and the other highest p_{T} jet are considered, and in the zero b-tag region the two highest p_{T} jets are used.

Boosted decision trees (BDTs) are used in the analysis to improve the separation of signals from background processes. Several variables that provide good discrimination between signal and background are used as inputs to the BDT: the invariant mass of the di-Higgs system (m_{hh}), reconstructed from the di-tau and di-b-jet system while using a 125 GeV Higgs mass constraint; the invariant mass of the di-tau system calculated using the MMC ($m_{\tau\tau}^{\text{MMC}}$); the invariant mass of the di-b-jet system (m_{bb}); the ΔR between the visible tau decay products ($\Delta R(\tau,\tau)$); the ΔR between the two b-jets ($\Delta R(b,b)$). The transverse mass between the lepton and the $E_{\mathrm{T}}^{\text{miss}}$ ($m_{\mathrm{T}}^{W} = \sqrt{2p_{\mathrm{T}}^{\ell}E_{\mathrm{T}}^{\text{miss}}(1-\cos\Delta\phi)}$) is used in $\tau_\ell\tau_{\text{had}}$ channel BDTs

and the $E_{\mathrm{T}}^{\mathrm{miss}}\phi$ centrality, defined as $E_{\mathrm{T}}^{\mathrm{miss}}\phi$ centrality $= (A + B)/(\sqrt{A^2 + B^2})$, where A and B are given by $A = (\sin(\phi_{E_{\mathrm{T}}^{\mathrm{miss}}} - \phi_{\tau_2}))/(\sin(\phi_{\tau_1} - \phi_{\tau_2}))$, $B = (\sin(\phi_{\tau_1} - \phi_{E_{\mathrm{T}}^{\mathrm{miss}}}))/(\sin(\phi_{\tau_1} - \phi_{\tau_2}))$, is used in the $\tau_{\mathrm{had}}\tau_{\mathrm{had}}$ channel and for the non-resonant search in the $\tau_\ell\tau_{\mathrm{had}}$ channel. The resonant search in the $\tau_\ell\tau_{\mathrm{had}}$ channel additionally includes as inputs to the BDT the following variables which help to improve separation from backgrounds at high mass: the $\Delta\phi$ angle between the two reconstructed 125 GeV Higgs bosons ($\Delta\phi$(h, h)) where the di-tau direction is taken from the MMC fit; the difference in p_{T} between the light lepton and the visible hadronic tau decay products ($\Delta p_{\mathrm{T}}(\ell, \tau)$); the sub-leading b-jet p_{T}.

When training on resonant signal samples (2HDM, Graviton), separate BDTs are trained for each signal mass point, where the signal model combines the target resonant mass and its two neighboring mass points so as to be sensitive to signal masses between the generated grid.

The dominant background processes – $t\bar{t}$ with real tau lepton decays and $Z/\gamma^* \to \tau\tau$ produced in association with heavy flavour jets (bb, bc, cc) – are normalised using control regions in data. Backgrounds in which the reconstructed hadronic taus are faked by jets (so-called 'fake taus') are estimated using data-driven methods. For the $\tau_\ell\tau_{\mathrm{had}}$ final state, fake-tau background contributions from $t\bar{t}$, W+jets and multi-jet processes are estimated using an inclusive fake-factor method. Background distributions are taken from control regions where τ_{had} candidates that are close to but fail the BDT identification requirements are selected. These distributions are scaled with a fake-factor that is determined by a comparison between all backgrounds and data in the control regions, following a technique similar to that described in Ref. [41]. For the $\tau_{\mathrm{had}}\tau_{\mathrm{had}}$ final state the W+jets and $t\bar{t}$ backgrounds are estimated from MC, where the fake-tau $t\bar{t}$ contribution is corrected from data by measuring the probability for a jet from a hadronic W-boson decay to be reconstructed as a hadronic tau using the technique described in Ref. [41]. The background predictions are compared to data in the 0, 1 and 2 b-tag regions after applying the event selection are found to be in good agreement.

All other background processes are estimated using simulations.

The uncertainty on the integrated luminosity of the dataset is 3.2% [42]. This systematic uncertainty is applied in a correlated way to all signal and background processes with the exception of fake-tau backgrounds that are estimated entirely from data.

Uncertainties are taken into account for the electron trigger, identification and reconstruction efficiencies, and for uncertainties associated with the isolation requirements. Uncertainties are also taken into account for muon p_{T}, identification efficiency and trigger efficiency. The size of the systematic uncertainties related to electron and muon objects is small compared to those related to taus and jets.

The tau energy scale and identification efficiency is corrected in MC to provide better agreement with data. Systematic uncertainties are included for the tau-electron overlap removal, the tau trigger, and the tau reconstruction. Among the trigger, reconstruction, identification and electron overlap removal systematics, none of the variations exceeds a 5% shape change on the final BDT.

The jet energy scale (JES) uncertainty depends on p_{T} and η and takes into account uncertainties due to pile-up effects. An uncertainty on the jet energy resolution (JER) is taken into account. Uncertainties on the energy scale and resolution of the electrons, muons, jets and taus are propagated to the calculation of the $E_{\mathrm{T}}^{\mathrm{miss}}$, which also has additional dedicated uncertainties on the scale, resolution, and reconstruction efficiency of tracks not associated to any of the reconstructed objects, along with the modelling of the underlying event. The fractional impact of the combined jet and $E_{\mathrm{T}}^{\mathrm{miss}}$uncertainties on the best-fit signal strength ($\hat{\mu}$) is ±0.07 [TODO: update].

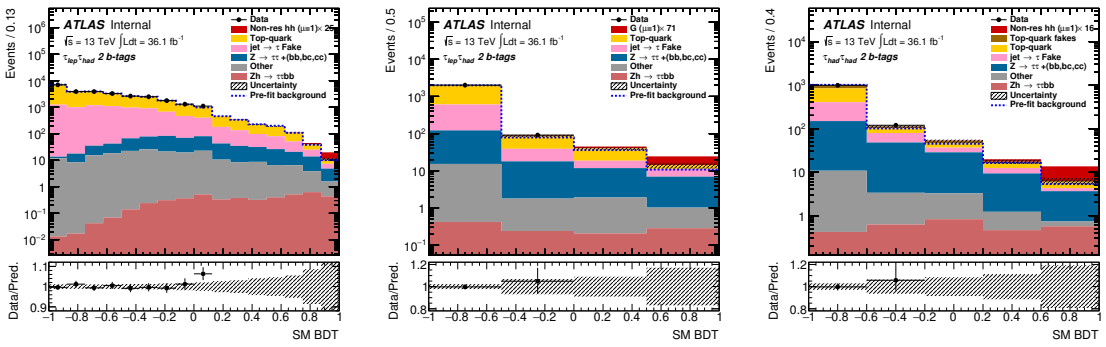

(a) $\tau_\ell\tau_{\text{had}}$ SLT channel (b) $\tau_\ell\tau_{\text{had}}$ LTT channel (c) $\tau_{\text{had}}\tau_{\text{had}}$channel

Figure 1: Distribution of the BDT output for non-resonant di-Higgs production in the $\tau_\ell\tau_{\text{had}}$ SLT (left) and LTT (centre) channels, and $\tau_{\text{had}}\tau_{\text{had}}$ channel (right). Distributions are shown after a fit to a background-only hypothesis.

Correction factors to account for flavour-tagging efficiency differences between simulation and data are measured separately for b, c, and light-flavour jets [39]. All three correction factors have many sources of uncertainty and are decomposed into uncorrelated components, which are then treated independently. The fractional impact of b-tagging uncertainties on the best-fit signal strength ($\hat{\mu}$) is ±0.06 [TODO: update].

[TODO: Add a note on the size of stat uncertainaties and background modeling uncertainties.]

The BDT output score is used as the discriminating variable for all channels and signals. The binning for the output BDT score distributions is optimised to ensure that the background uncertainty is kept to below 40% of the signal fraction. If there is no signal in a bin the uncertainty is required to be below 1%. In addition a minimum number of five events in each bin is required. To assess the compatibility of the SM background-only hypothesis with the observations in the signal regions, a profile likelihood ratio test is performed. All sources of systematic and statistical uncertainties on the signal and background modelling are implemented as deviations from the nominal model scaled by nuisance parameters that are profiled in the fit. The observed number of events are found to be compatible with the fitted number of background events. As no significant excess over the expected background from SM processes is observed, the data are used to set upper limits on resonant and non-resonant Higgs pair-production at 95% CL. The results are obtained from a profile likelihood ratio test following the CLs prescription [43].

Good agreement between data and expected background is observed in all channels and for all signal models. The BDT responses for the non-resonant search after performing the fit when assuming a background-only hypothesis are shown in figure1.

Upper limits on the cross-section for non-resonant di-Higgs production are set and interpreted as multiples of the SM prediction. The results are presented in table 1. The results for resonance searches are presented as exclusion limits on the hh-production cross-section, given as a function of the resonance mass. The expected limits for 2HDM and graviton signal models are shown in figure **??** for the $\tau_\ell\tau_{\text{had}}$ channels, the $\tau_{\text{had}}\tau_{\text{had}}$ channel, and the combination.

In the 2HDM interpretation, heavy Higgs bosons are excluded at 95% CL in the mass range A < m_{H} < B GeV (assuming <some 2HDM model paramaters>). Gravitons are excluded at 95% CL in the mass range C < m_{G} < D GeV (assuming <some RS graviton model parameters>). Non-resonant di-Higgs production is excluded for cross-sections up to XX pb (YY times the SM prediction).

		Observed	-2σ	-1σ	Expected	+1σ	+2σ
$\tau_\ell\tau_{\text{had}}$ (SLT)	σ [pb]		0.47	0.63	0.87	1.21	1.63
	$\sigma/\sigma_{\text{SM}}$		14.02	18.81	26.10	36.33	48.70
$\tau_\ell\tau_{\text{had}}$ (LTT)	σ [pb]		1.26	1.69	2.35	3.27	4.48
	$\sigma/\sigma_{\text{SM}}$		37.70	50.62	70.25	97.77	131.06
$\tau_\ell\tau_{\text{had}}$ Combined	σ [pb]		0.44	0.59	0.82	1.14	1.52
	$\sigma/\sigma_{\text{SM}}$		13.11	17.60	24.43	33.99	45.57
$\tau_{\text{had}}\tau_{\text{had}}$	σ [pb]		0.28	0.38	0.52	0.73	0.98
	$\sigma/\sigma_{\text{SM}}$		8.42	11.31	15.69	21.84	29.28

Table 1: Upper limits on the production cross-section for non-resonant di-Higgs production at 95% CL.

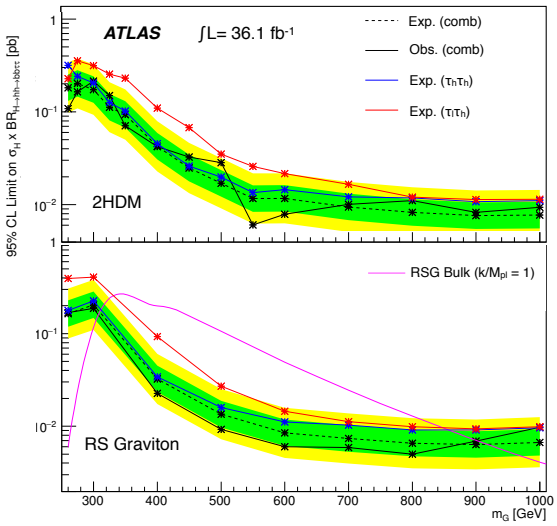

Figure 2: Expected limits at 95% C.L. on the cross-sections of the 2HDM $H \to hh$ (top) and RS $G \to hh$ (bottom) processes when combining $\tau_\ell\tau_{\text{had}}$ and $\tau_{\text{had}}\tau_{\text{had}}$ channels. The expected cross-section for RS graviton production (assuming c = 1.0) is also shown in the relevant plots. [TODO: Make the plot labels larger]

The results significantly improve upon the ATLAS Run 1 results, where 20.1 fb^{-1} data with $\sqrt{s}$ = 8 TeV was used to search for di-Higgs production in the $bb\tau\tau$ ($\tau_\ell\tau_{\text{had}}$) final state. The results also set stronger limits on Higgs pair-production than the latest CMS results in this channel (using 35.9 fb^{-1} data at $\sqrt{s}$ =13 TeV). It should be noted that the limits on non-resonant di-Higgs production are set on a BDT trained against the full SM di-Higgs signal from both the top loop production process and the Higgs self-interaction and, because of the kinematics of the top loop production process, the BDT is more sensitive to signal from this production.

References

[1] ATLAS Collaboration, *Observation of a new particle in the search for the Standard Model Higgs boson with the ATLAS detector at the LHC*, Phys. Lett. **B 716** (2012) 1, arXiv: 1207.7214 [hep-ex].

[2] CMS Collaboration, *Observation of a new boson at a mass of 125 GeV with the CMS experiment at the LHC*, Phys. Lett. **B 716** (2012) 30, arXiv: 1207.7235 [hep-ex].

[3] G. Branco et al., *Theory and phenomenology of two-Higgs-doublet models*, Phys. Rept. **516** (2012) 1, arXiv: 1106.0034 [hep-ph].

[4] K. Agashe et al., *Warped Gravitons at the LHC and Beyond*, Phys. Rev. **D76** (2007) 036006, arXiv: hep-ph/0701186 [hep-ph].

[5] A. L. Fitzpatrick et al., *Searching for the Kaluza-Klein Graviton in Bulk RS Models*, JHEP **09** (2007) 013, arXiv: hep-ph/0701150 [hep-ph].

[6] ATLAS Collaboration, *The ATLAS Experiment at the CERN Large Hadron Collider*, JINST **3** (2008) S08003.

[7] ATLAS Collaboration, *Searches for Higgs boson pair production in the $hh \to bb\tau\tau, \gamma\gamma WW^*, \gamma\gamma bb, bbbb$ channels with the ATLAS detector*, Phys. Rev. **D92** (2015) 092004, arXiv: 1509.04670 [hep-ex].

[8] ATLAS Collaboration, *Search for Higgs boson pair production in the $b\bar{b}b\bar{b}$ final state from pp collisions at $\sqrt{s} = 8$ TeVwith the ATLAS detector*, Eur. Phys. J. **C75** (2015) 412, arXiv: 1506.00285 [hep-ex].

[9] ATLAS Collaboration, *Search For Higgs Boson Pair Production in the $\gamma\gamma b\bar{b}$ Final State using pp Collision Data at $\sqrt{s} = 8$ TeV from the ATLAS Detector*, Phys. Rev. Lett. **114** (2015) 081802, arXiv: 1406.5053 [hep-ex].

[10] CMS Collaboration, 'Search for pair production of Higgs bosons in the two tau leptons and two bottom quarks final state using proton-proton collisions at $\sqrt{s} = 13$ TeV', tech. rep. CMS-PAS-HIG-17-002, CERN, 2017, URL: https://cds.cern.ch/record/2256096.

[11] J. Alwall et al., *MadGraph 5 : Going Beyond*, JHEP **06** (2011) 128, arXiv: 1106.0522 [hep-ph].

[12] T. Sjöstrand, S. Mrenna and P. Skands, *A Brief Introduction to PYTHIA 8.1*, Comput. Phys. Commun. **178** (2008) 852, arXiv: 0710.3820 [hep-ph].

[13] ATLAS Collaboration, 'ATLAS Run 1 Pythia8 tunes', tech. rep., 2014, URL: https://cds.cern.ch/record/1966419.

[14] Ball, Richard D. and others, *Parton distributions with LHC data*, Nucl. Phys. **B867** (2013) 244, arXiv: 1207.1303 [hep-ph].

[15] J. Alwall et al, *The automated computation of tree-level and next-to-leading order differential cross sections, and their matching to parton shower simulations*, JHEP **07** (2014) 079, arXiv: 1405.0301 [hep-ph].

[16] M. Bahr et al., *Herwig++ Physics and Manual*, Eur. Phys. J. C **58** (2008) 639, arXiv: 0803.0883 [hep-ph].

[17] S. Borowka et al., *Higgs Boson Pair Production in Gluon Fusion at Next-to-Leading Order with Full Top-Quark Mass Dependence*, Phys. Rev. Lett. **117** (2016) 012001, [Erratum: Phys. Rev. Lett.117,no.7,079901(2016)], arXiv: 1604.06447 [hep-ph].

[18] S. Borowka et al., *Full top quark mass dependence in Higgs boson pair production at NLO*, JHEP **10** (2016) 107, arXiv: 1608.04798 [hep-ph].

[19] S. Alioli et al., *NLO Higgs boson production via gluon fusion matched with shower in POWHEG*, JHEP **04** (2009) 002, arXiv: 0812.0578 [hep-ph].

[20] P. Artoisenet et al., *Automatic spin-entangled decays of heavy resonances in Monte Carlo simulations*, JHEP **1303** (2013) 015, arXiv: 1212.3460 [hep-ph].

[21] T. Sjöstrand, S. Mrenna and P. Skands, *PYTHIA 6.4 physics and manual*, JHEP **05** (2006) 026, arXiv: hep-ph/0603175 [hep-ph].

[22] P. Z. Skands, *Tuning Monte Carlo Generators: The Perugia Tunes*, Phys. Rev. **D82** (2010) 074018, arXiv: 1005.3457 [hep-ph].

[23] D. J. Lange, *The EvtGen particle decay simulation package*, Nucl. Instrum. Meth. **A462** (2001) 152.

[24] M. Czakon et al., *Constraints on the gluon PDF from top quark pair production at hadron colliders*, JHEP **07** (2013) 167, arXiv: 1303.7215 [hep-ph].

[25] T. Gleisberg et al., *Event generation with SHERPA 1.1*, JHEP **02** (2009) 007, arXiv: 0811.4622 [hep-ph].

[26] T. Gleisberg and S. Höche, *Comix, a new matrix element generator*, JHEP **12** (2008) 039, arXiv: 0808.3674 [hep-ph].

[27] F. Cascioli, P. Maierhofer and S. Pozzorini, *Scattering Amplitudes with Open Loops*, Phys. Rev. Lett. **108** (2012) 111601, arXiv: 1111.5206 [hep-ph].

[28] S. Schumann and F. Krauss, *A Parton shower algorithm based on Catani-Seymour dipole factorisation*, JHEP **03** (2008) 038, arXiv: 0709.1027 [hep-ph].

[29] S. Höche et al., *QCD matrix elements + parton showers: The NLO case*, JHEP **04** (2013) 027, arXiv: 1207.5030 [hep-ph].

[30] ATLAS Collaboration, *Measurement of the Z/γ^* boson transverse momentum distribution in pp collisions at $\sqrt{s} = 7$ TeV with the ATLAS detector*, JHEP **2014** (2014) 55, arXiv: 1406.3660 [hep-ex].

[31] GEANT4 Collaboration, S. Agostinelli et al., *GEANT4 - a simulation toolkit*, Nucl. Instrum. Meth. **A 506** (2003) 250.

[32] ATLAS Collaboration, *The ATLAS simulation infrastructure*, Eur. Phys. J. **C 70** (2010) 823, arXiv: 1005.4568 [physics.ins-det].

[33] ATLAS Collaboration, *Electron reconstruction and identification efficiency measurements with the ATLAS detector using the 2011 LHC proton-proton collision data*, Eur.Phys.J. **C74** (2014) 2941, arXiv: 1404.2240 [hep-ex].

[34] ATLAS Collaboration, *Muon reconstruction performance of the ATLAS detector in proton–proton collision data at $\sqrt{s}$ =13 TeV*, Eur. Phys. J. **C76** (2016) 292, arXiv: 1603.05598 [hep-ex].

[35] ATLAS Collaboration, *Measurement of the tau lepton reconstruction and identification performance in the ATLAS experiment using pp collisions at $\sqrt{s}$ = 13 TeV*, (2017), URL: https://cds.cern.ch/record/2261772.

[36] ATLAS Collaboration, 'Reconstruction, Energy Calibration, and Identification of Hadronically Decaying Tau Leptons in the ATLAS Experiment for Run-2 of the LHC', tech. rep. ATL-PHYS-PUB-2015-045, CERN, 2015, URL: https://cds.cern.ch/record/2064383.

[37] ATLAS Collaboration, *Identification and energy calibration of hadronically decaying tau leptons with the ATLAS experiment in pp collisions at $\sqrt{s}$=8 TeV*, Eur. Phys. J. **C 75** (2015) 303, arXiv: 1412.7086 [hep-ex].

[38] A. Elagin et al., *A New Mass Reconstruction Technique for Resonances Decaying to di-tau*, Nucl. Instrum. Meth. **A 654** (2011) 481, arXiv: 1012.4686 [hep-ex].

[39] ATLAS Collaboration, *Performance of b-Jet Identification in the ATLAS Experiment*, JINST **11** (2016) P04008, arXiv: 1512.01094 [hep-ex].

[40] ATLAS Collaboration, 'Optimisation of the ATLAS *b*-tagging performance for the 2016 LHC Run', tech. rep. ATL-PHYS-PUB-2016-012, CERN, 2016, URL: https://cds.cern.ch/record/2160731.

[41] ().

[42] ATLAS Collaboration, *Luminosity determination in pp collisions at $\sqrt{s}$ = 8 TeV using the ATLAS detector at the LHC*, Eur. Phys. J. **C76** (2016) 653, arXiv: 1608.03953 [hep-ex].

[43] A. L. Read, *Presentation of search results: the CL s technique*, Journal of Physics G: Nuclear and Particle Physics **28** (2002) 2693, URL: http://stacks.iop.org/0954-3899/28/i=10/a=313.